

Dynamical Properties of Internal Shocks Revisited

Asaf Pe'er ¹, Killian Long ¹, and Piergiorgio Casella ²

ABSTRACT

Internal shocks between propagating plasma shells, originally ejected at different times with different velocities are believed to play a major role in dissipating the kinetic energy, thereby explaining the observed lightcurve and spectra in a large range of transient objects. Even if initially the colliding plasmas are cold, following the first collision the plasma shells are substantially heated, implying that in a scenario of multiple collisions, most collisions take place between plasmas of non-zero temperatures. Here, we calculate the dynamical properties of plasmas resulting from collision between arbitrarily hot plasma shells, moving at arbitrary speeds. We provide simple analytical expressions valid for both the ultra-relativistic and Newtonian velocities, for both hot and cold plasmas. We derive the minimum criteria required for the formation of the two-shock wave system, and show that in the relativistic limit, the minimum Lorentz factor is proportional to the square root of the ratio of the initial plasmas enthalpies. We provide basic scaling laws of synchrotron emission from both the forward and reverse shock waves, and show how these can be used to deduce the properties of the colliding shells. Finally, we discuss the implications of these results in the study of several astronomical transients, such as x-ray binaries, radio loud quasars and gamma-ray bursts.

1. Introduction

Lightcurves of many astronomical transients that are characterized by strong outflows (jets) show substantial variability, observed on timescales as fast as millisecond and possibly even faster. Several examples include blazars (Marscher 1980), gamma-ray bursts (GRBs; Norris et al. 1996) and x-ray binaries (XRBs; Fender 2001). A leading model proposed to explain this variable lightcurve is the internal shocks model. The basic idea is that variability within the inner engine results in fluctuations in the ejection of plasmas. Thus, the ejected

¹Physics Department, University College Cork, Cork, Ireland

²INAF, Osservatorio Astronomico di Roma, Via Frascati 33, I-00078 Monteporzio Catone, Italy

material propagates as a collection of “plasma shells”, each accelerated and propagates at some terminal velocity which is independent on the terminal velocities of the other plasma shells. At a second stage, shells that were ejected at later times but with faster speeds, catch up with the slower shells ahead. The collision between the plasma shells results in the formation of two shock waves (forward and reverse) that propagate, respectively, into the slow and fast shells. These shock waves dissipate part of the shells’ kinetic energy, which is then radiated away. Following the collision, the colliding shells are assumed to merge and continue propagating together (i.e., the collision is considered as a plastic collision), and are therefore subject to a subsequent collision with a third incoming, faster shell. This scenario of multiple collisions therefore results in the observed variable lightcurve.

Such models were proposed to explain the knots in active galactic nuclei [AGN] jets (Rees 1978). They have been in wide use since the 1990’s in explaining the rapid variability observed during the prompt phase of many GRBs (e.g., Rees & Meszaros 1994; Fenimore et al. 1996; Sari & Piran 1997; Kobayashi et al. 1997; Daigne & Mochkovitch 1998; Panaitescu et al. 1999; Ramirez-Ruiz & Fenimore 2000; Guetta et al. 2001; Mészáros et al. 2002; Nakar & Piran 2002; Kino et al. 2004; Cantó et al. 2013), as well as in blazars (Sikora et al. 1994; Ghisellini 1999; Spada et al. 2001; Böttcher & Dermer 2010; Mimica & Aloy 2010). In recent years, similar models were applied in the study of variable emission from XRBs (Kaiser et al. 2000; Miller-Jones et al. 2005; Jamil et al. 2010; Malzac 2013, 2014; Drappeau et al. 2015) as well as tidal disruption events (Wang & Cheng 2012); See Pe’er (2014) for a review. Indeed, the hydrodynamical properties of the shock waves as well as the colliding shells had long been investigated in the non-relativistic as well as in the relativistic regimes (Blandford & McKee 1976; Sari & Piran 1995).

One thing in common to these models is that a detailed description of the shocked plasma conditions are calculated based on the assumption that the colliding plasmas are initially cold (Sari & Piran 1995). While the expanding plasma shells lose their energy adiabatically during the expansion, the shock waves formed in each collision substantially heat the plasma. Thus, even if initially the plasmas are cold, in a scenario of multiple collisions, in general the colliding plasmas are not expected to be cold. While this fact was considered by several authors in calculating the overall efficiency of energy conversion (Panaitescu et al. 1999; Beloborodov 2000; Spada et al. 2001; Guetta et al. 2001; Kino et al. 2004; Jamil et al. 2010), so far no detailed description of the shocked plasma properties was calculated in the general scenario of arbitrary hot plasmas colliding at arbitrary velocities.

Such calculation is of particular importance for two reasons. First, when arbitrary hot plasmas collide, the conditions for the formation of the two shock wave system are not always fulfilled. As a result, the amount of energy dissipated in such a collision can be substantially

smaller than if shock waves are formed. Second, even if shock waves are formed, the expected spectra depends on the energy density and energy per particle in the shocked region, which are in general different than in the cold plasma collision scenario (Zhang & Mészáros 2002). Thus, in order to provide accurate calculations of the expected lightcurve and spectra, the conditions at the shocked plasma needs to be determined.

In this work, we calculate the properties of the shocked plasma following the collision of arbitrarily hot plasma shells. We consider a simple 1-d model which enables us to provide simple analytic estimations of the thermodynamic properties of the shocked plasmas in the various regimes. As we show below, one needs to discriminate not only between the relativistic and non-relativistic scenarios, but the analytical solutions also depend on the energy densities of the plasmas. We thus discriminate between “cold”, “cool” and “hot” plasmas (see definitions in §2 below). We derive the minimum criteria for the formation of such shocks in the different scenarios, as well as the properties (velocity, energy density and energy per particle) of the shocked plasma. In §3 we provide a full numerical solution, which can be used for arbitrary plasma properties, and further serves to validate and demonstrate the analytical approximations in the different regimes. In §4 we discuss observational consequences of the model, and in particular we show that the efficiency in energy conversion is different than previous claims, due to the need to include a pressure term. We further demonstrate how the properties of the synchrotron emission can be used to probe the properties of the colliding shells, before summarizing in §5.

2. Basic Setup

We consider a slab of (non-magnetized) plasma shell (“slow shell”), that propagates at some arbitrary speed $\beta_1 = v_1/c$ (corresponding Lorentz factor Γ_1) in the lab frame. A second plasma shell (“fast shell”), that propagates at velocity $\beta_4 > \beta_1$ collides with the slow shell. At sufficiently high β_4 , two shock waves are formed as a result of the collision: a forward shock propagating into the slow shell, and a reverse shock propagating into the fast shell. A contact discontinuity separates the shocked slow shell material from the shocked fast shell material.

Following the collision, there are four different regimes: (1) the slow shell, (2) the shocked slow shell, (3) the shocked fast shell, and (4) the fast shell material. The velocities of the four regimes are β_i , ($i = 1..4$) and the corresponding Lorentz factors $\Gamma_i = (1 - \beta_i)^{-1/2}$. The thermodynamical quantities: n_i , e_i , p_i and $\omega_i = e_i + p_i$ (number density, internal energy density, pressure and enthalpy, respectively) are measured in each of the fluid’s (shells) rest frame. We further denote the speed of the forward and reverse shock waves by β_{fs} , β_{rs} ,

respectively (corresponding Lorentz factors Γ_{fs} , Γ_{rs}).

The system considered therefore contains a total of 18 free parameters (β_i, n_i, e_i, p_i [$i = 1..4$], β_{fs} , β_{rs}). The shock jump conditions: conservations of particle, energy and momentum flux densities at each shock wave provide six equations. Two more equations are provided by equating the pressures and velocities along the contact discontinuity. Additional four equations of state, of the form $p_i = (\hat{\gamma}_i - 1)(e_i - n_i)$, where $\hat{\gamma}_i$ is the adiabatic index in region i , complete a total of 12 equations connecting the velocities and thermodynamic quantities in all four regimes. Thus, by specifying a total of six boundary conditions, namely the initial velocities, number and energy densities in the slow and fast plasma shells ($\beta_1, \beta_4, n_1, n_4, e_1, e_4$), the velocities and thermodynamic properties of all four regions of the system are fully determined.¹

We provide below a complete solution in the planar case. Clearly, in the most general scenario such a solution can only be determined numerically. However, simple analytical solutions exist in the limiting cases of relativistic ($\Gamma_4 \gg \Gamma_1$) as well as Newtonian ($\beta_4, \beta_1 \ll 1$) plasma velocities. We thus first consider the analytical solutions, before providing a few examples of the full numerical solution in §3 below.

2.1. Analytical Solution: Basic Equations

For simplicity, we assume in the calculations below that the slow plasma is at rest ($\beta_1 = 0$, $\Gamma_1 = 1$). This can be viewed both as a specific case, but equally as conducting the calculations in the rest frame of the slow plasma shell. Towards the end of this section, we transform the derived results to the lab frame, in which $\Gamma_1 \geq 1$ is arbitrary. Thus, in the calculations below, Γ_2 is the Lorentz factor of the shocked slow plasma (region (2)) in the rest frame of region (1), etc.

The forward shock jump conditions follow from the continuity of energy ($T^{01} = \omega\Gamma^2\beta$), momentum ($T^{11} = \omega\Gamma^2\beta^2 + p$) and particle ($n\Gamma\beta$) flux densities in the shock frame. Here, $T^{\mu\nu} = \omega u^\mu u^\nu + p\eta^{\mu\nu}$ is the stress- energy tensor, u^μ is the 4-velocity and $\eta^{\mu\nu}$ is the metric tensor. In their most general form, the forward shock jump conditions can be put in the form (Blandford & McKee 1976; Wiersma 2007)

$$\frac{e_2}{n_2} = \Gamma_2 \frac{\omega_1}{n_1} - \frac{p_1}{n_2}, \quad (1)$$

¹We assume that the conditions are homogeneous within each regime. This approximation is reasonable as long as the initial colliding shells are not too wide. It can easily be justified in the shocked regions, which are sub-sonic.

$$p_2 - p_1 = \frac{(\Gamma_2 \beta_2)^2 n_2 \omega_1}{n_2 - \Gamma_2 n_1} \quad (2)$$

Similarly, the reverse shock jump conditions are written as

$$\frac{e_3}{n_3} = \bar{\Gamma}_3 \frac{\omega_4}{n_4} - \frac{p_4}{n_3}, \quad (3)$$

$$p_3 - p_4 = \frac{(\bar{\Gamma}_3 \bar{\beta}_3)^2 n_3 \omega_4}{n_3 - \bar{\Gamma}_3 n_4}. \quad (4)$$

Here, $\bar{\Gamma}_3 = \Gamma_3 \Gamma_4 (1 - \beta_3 \beta_4)$ is the Lorentz factor of the shocked material in region (3) relative to the unshocked fast shell in region (4), and $\bar{\beta}_3 = (1 - \bar{\Gamma}_3^{-2})^{1/2}$ is the corresponding velocity.

2.2. Relativistic collision

In the ultra-relativistic case, we consider the scenario where $\Gamma_4 \gg \Gamma_2 = \Gamma_3 \gg 1$. Under this assumption,

$$\bar{\Gamma}_3 \simeq \frac{1}{2} \left(\frac{\Gamma_4}{\Gamma_3} + \frac{\Gamma_3}{\Gamma_4} \right) \approx \frac{\Gamma_4}{2\Gamma_2}. \quad (5)$$

Since it is always true that $n_2 \geq n_1$ and $n_3 \geq n_4$, it is safe to neglect the second terms in equations 1 and 3. The pressures in regions (2) and (3) can therefore be written as

$$\begin{aligned} p_2 &= (\hat{\gamma}_2 - 1) n_2 \left(\frac{e_2}{n_2} - 1 \right) \simeq (\hat{\gamma}_2 - 1) n_2 \Gamma_2 \frac{\omega_1}{n_1}; \\ p_3 &\simeq (\hat{\gamma}_3 - 1) \omega_4 \bar{\Gamma}_3 \frac{n_3}{n_4}. \end{aligned} \quad (6)$$

Using these results in Equations 2, 4, and neglecting $p_1 \ll p_2$ as well as $p_4 \ll p_3$ (which is correct in the ultra-relativistic limit), one obtains

$$\frac{n_2}{n_1} = \frac{\hat{\gamma}_2}{\hat{\gamma}_2 - 1} \Gamma_2; \quad \frac{n_3}{n_4} = \frac{\hat{\gamma}_3}{\hat{\gamma}_3 - 1} \bar{\Gamma}_3. \quad (7)$$

In the relativistic limit, the adiabatic indices are $\hat{\gamma}_2 = \hat{\gamma}_3 = 4/3$. Using these results, as well as the approximation derived in Equation 5 in Equation 6, the requirement $p_2 = p_3$ leads to

$$\Gamma_2 = \Gamma_3 \simeq \sqrt{\frac{\Gamma_4}{2}} \left(\frac{\omega_4}{\omega_1} \right)^{1/4}, \quad \bar{\Gamma}_3 \simeq \sqrt{\frac{\Gamma_4}{2}} \left(\frac{\omega_1}{\omega_4} \right)^{1/4}. \quad (8)$$

Using Equations 1, 3 and 7, the energy per particle and the energy densities in regions (2) and (3) are given by

$$\begin{aligned} \frac{e_2}{n_2} &\simeq \sqrt{\frac{\Gamma_4}{2}} \frac{\omega_1^{3/4} \omega_4^{1/4}}{n_1}; & \frac{e_3}{n_3} &\simeq \sqrt{\frac{\Gamma_4}{2}} \frac{\omega_1^{1/4} \omega_4^{3/4}}{n_4}; \\ e_2 = e_3 &\simeq \frac{\hat{\gamma}_2}{\hat{\gamma}_2 - 1} \frac{\Gamma_4}{2} \omega_1^{1/2} \omega_4^{1/2} = 2\Gamma_4 \omega_1^{1/2} \omega_4^{1/2}, \end{aligned} \quad (9)$$

where in the last line we took $\hat{\gamma}_2 = \hat{\gamma}_3 = 4/3$.

The results derived in Equation 9 can further be used to set a minimum criteria on the Lorentz factor of the fast shell, Γ_4 that enables the existence of the two shock system if the colliding plasma shells are initially hot. Writing $e_i = \omega_i/\hat{\gamma}_i + (\hat{\gamma}_i - 1)n_i/\hat{\gamma}_i \approx \omega_i/\hat{\gamma}_i$, the requirements $e_2 \geq e_1$ and $e_3 > e_4$ are translated into the criteria

$$\begin{aligned} \Gamma_4 &\geq 2 \frac{\hat{\gamma}_2 - 1}{\hat{\gamma}_1 \hat{\gamma}_2} \sqrt{\frac{\omega_1}{\omega_4}} = \frac{3}{8} \sqrt{\frac{\omega_1}{\omega_4}}, \\ \Gamma_4 &\geq 2 \frac{\hat{\gamma}_3 - 1}{\hat{\gamma}_4 \hat{\gamma}_3} \sqrt{\frac{\omega_4}{\omega_1}} = \frac{3}{8} \sqrt{\frac{\omega_4}{\omega_1}}, \end{aligned} \rightarrow \Gamma_4 \geq \frac{3}{8} \max \left\{ \sqrt{\frac{\omega_4}{\omega_1}}, \sqrt{\frac{\omega_1}{\omega_4}} \right\}, \quad (10)$$

where we took $\hat{\gamma}_i = 4/3$ in all four regimes, which is valid for hot plasmas. This minimum value of the Lorentz factor can be understood as follows: As the Lorentz factor of the fast shell (Γ_4) decreases, eventually either the forward or reverse shock ceases to be relativistic, and the amount of energy dissipated from the (initially hot) plasma shells decreases. When this criterion is met, (at least) one of the two shock waves ceases to exist. Instead, a rarefaction wave will be created and propagate into the hot plasma, while the second shock wave could still exist.

Finally, we note that a Lorentz transformation to the *lab frame*, in which $\Gamma_1^L \equiv \Gamma_1 \gg 1$, yields $\Gamma_2^L = \Gamma_1 \Gamma_2 (1 + \beta_1 \beta_2) \simeq 2\Gamma_1 \Gamma_2$, and similarly $\Gamma_4^L \simeq 2\Gamma_1 \Gamma_4$. The Lorentz factor of the shocked plasmas are therefore given by (Equation 8),

$$\Gamma_2^L = \sqrt{\Gamma_1^L \Gamma_4^L} \left(\frac{\omega_4}{\omega_1} \right)^{1/4}. \quad (11)$$

2.3. Newtonian collision

We next consider the Newtonian (non-relativistic) case, in which the relative motion between the two colliding shells is non- or trans-relativistic at most. We do allow, though, the colliding plasmas to be arbitrarily hot. Similar to the relativistic treatment, we initially assume $\Gamma_1 = 1$.

When writing the energy density in region (1) as $e_1 = n_1 + \epsilon_1$, the forward shock jump conditions (equations 1, 2) can be written as a quadratic equation in the ratio of the proper densities at both sides of the forward shock wave,

$$\left(\frac{n_2}{n_1} \right)^2 \left[\Gamma_2 \left(1 + \hat{\gamma}_1 \frac{\epsilon_1}{n_1} \right) - 1 \right] - \left(\frac{n_2}{n_1} \right) \left[\left(1 + \hat{\gamma}_1 \frac{\epsilon_1}{n_1} \right) \left(2 + \frac{\hat{\gamma}_2}{\hat{\gamma}_2 - 1} \Gamma_2^2 \beta_2^2 \right) - (\Gamma_2 + 1) \right] + \hat{\gamma}_1 \Gamma_2 \frac{\epsilon_1}{n_1} = 0 \quad (12)$$

(with a similar equation holding for the reverse shock). Note that Equation 12 is exact for all velocities. In order to obtain useful approximation in the Newtonian regime, one needs

to (i) approximate $\Gamma_2 \simeq 1 + \beta_2^2/2$; and (ii) discriminate between different regimes, based on the value of ϵ_1 : hot, cool and cold.

In the **hot regime**, $\epsilon_1/n_1 \gg 1$. The ratio of densities at both sides of the shock waves becomes

$$\left(\frac{n_2}{n_1}\right)_{\text{hot}} \simeq 1 + \frac{\beta_2}{\sqrt{\hat{\gamma}_2 - 1}} + \frac{\beta_2^2}{2(\hat{\gamma}_2 - 1)} = 1 + \sqrt{3}\beta_2 + \frac{3}{2}\beta_2^2 \quad (13)$$

where we took $\hat{\gamma}_1 = \hat{\gamma}_2 \simeq 4/3$ in the last equality. Using this result in Equation 1, the energy density in region (2) is given by

$$e_2 \simeq \epsilon_1 \left(1 + \frac{\hat{\gamma}_1}{\sqrt{\hat{\gamma}_2 - 1}}\beta_2 + \frac{\hat{\gamma}_1\hat{\gamma}_2}{2(\hat{\gamma}_2 - 1)}\beta_2^2\right) = \epsilon_1 \left(1 + \frac{4}{\sqrt{3}}\beta_2 + \frac{8}{3}\beta_2^2\right). \quad (14)$$

Clearly, a similar equation holds for the energy density in region (3).

In the opposite, **cool / cold** limit, namely $\epsilon_1/n_1 \ll 1$, we proceed as follows. First, in the non-relativistic limit, $\beta_2 \ll 1$, the ratio of densities derived from the shock jump conditions (Equation 12) can be put in the form

$$\left(\frac{n_2}{n_1}\right)^2 \left[\frac{\beta_2^2}{2} + \hat{\gamma}_1 \frac{\epsilon_1}{n_1} \left(1 + \frac{\beta_2^2}{2}\right)\right] - \left(\frac{n_2}{n_1}\right) \left[\left(\frac{\hat{\gamma}_2 + 1}{\hat{\gamma}_2 - 1}\right) \frac{\beta_2^2}{2} + 2\hat{\gamma}_1 \frac{\epsilon_1}{n_1} \left(1 + \frac{\hat{\gamma}_2}{\hat{\gamma}_2 - 1} \frac{\beta_2^2}{2}\right)\right] + \hat{\gamma}_1 \frac{\epsilon_1}{n_1} \left(1 + \frac{\beta_2^2}{2}\right) = 0. \quad (15)$$

We next discriminate between the **cool** case, in which $\epsilon_1/n_1 \gg \beta_2^2$, and the opposite, **cold** case, in which $\epsilon_1/n_1 \ll \beta_2^2$. In the **cool** scenario, the ratio of densities and the energy density in region (2) are given by

$$\begin{aligned} \left(\frac{n_2}{n_1}\right)_{\text{cool}} &\simeq 1 + \frac{1}{\sqrt{\hat{\gamma}_1(\hat{\gamma}_2 - 1)} \frac{\epsilon_1}{n_1}} \beta_2 + \frac{3 - \hat{\gamma}_2}{4\hat{\gamma}_1(\hat{\gamma}_2 - 1) \frac{\epsilon_1}{n_1}} \beta_2^2, \\ (e_2)_{\text{cool}} &\simeq n_1 \left[1 + \frac{\epsilon_1}{n_1} + \frac{1}{\sqrt{\hat{\gamma}_2 - 1}} \left(\sqrt{\hat{\gamma}_1 \frac{\epsilon_1}{n_1}} + \frac{1}{\sqrt{\hat{\gamma}_1 \frac{\epsilon_1}{n_1}}}\right) \beta_2\right]. \end{aligned} \quad (16)$$

In this case, the value of the adiabatic index is not a-priori known (see discussion in section 3 below).

In the **cold** scenario, $\epsilon_1/n_1 \ll \beta_2^2$, similar calculation yields

$$\begin{aligned} \left(\frac{n_2}{n_1}\right)_{\text{cold}} &\simeq \left(\frac{\hat{\gamma}_2 + 1}{\hat{\gamma}_2 - 1}\right) + \frac{2\hat{\gamma}_1}{\hat{\gamma}_2 + 1} \frac{\epsilon_1}{n_1} - \frac{8\hat{\gamma}_1}{(\hat{\gamma}_2 + 1)(\hat{\gamma}_2 - 1)} \frac{\epsilon_1}{n_1 \beta_2^2} = 4 + \left(\frac{5}{4} - \frac{15}{2\beta_2^2}\right) \left(\frac{\epsilon_1}{n_1}\right), \\ (e_2)_{\text{cold}} &\simeq n_1 \left[\left(\frac{\hat{\gamma}_2 + 1}{\hat{\gamma}_2 - 1}\right) \left(1 + \frac{\beta_2^2}{2}\right) - \frac{8\hat{\gamma}_1}{(\hat{\gamma}_2 + 1)(\hat{\gamma}_2 - 1)} \left(\frac{\epsilon_1}{n_1 \beta_2^2}\right) + \frac{3\hat{\gamma}_1 + 1}{\hat{\gamma}_2 + 1} \left(\frac{\epsilon_1}{n_1}\right)\right] \\ &= n_1 \left[4 \left(1 + \frac{\beta_2^2}{2}\right) + \left(\frac{9}{4} - \frac{15}{2\beta_2^2}\right) \left(\frac{\epsilon_1}{n_1}\right)\right], \end{aligned} \quad (17)$$

where we used $\hat{\gamma}_1 = \hat{\gamma}_2 = 5/3$ in the last equality. We further point out that given an arbitrary value of $0 < (\epsilon_1/n_1) < 1$, for very small relative velocities between the plasma

shells the plasma can be considered as “cool”, while at higher velocities it can be regarded as “cold”.

The results presented in Equations 12 – 17 are of course symmetric with respect to the reverse shock, and are obtained by replacing quantities in regions (1), (2) with those in regions (4), (3), respectively, and exchanging β_2 with $\bar{\beta}_3 \simeq \beta_4 - \beta_2$. Using these replacements, one can use the requirement $p_2 = p_3$ to determine the shocked plasma velocity, $\beta_2 = \beta_3$ as a function of the colliding plasmas parameters (n_1, e_1, n_4 and e_4) as well as their relative velocities β_4 in the different regimes. The results of the various scenarios are summarized in Table 1.

The results in Table 1 can also be used to put constraints on the minimum relative velocities between the shells (β_4) that enables the formation of the double shock structure. These limits originate from the requirements (a) $\beta_2 \geq 0$ and (b) $\bar{\beta}_3 = \beta_4 - \beta_2 \geq 0$. In the first scenario considered in Table 1, that of interaction between two cold plasmas, β_2 is always smaller than β_4 and therefore there is no restriction: a double shock structure will always form, for each value of $\beta_4 > 0$. However, this is the exceptional case: in all other scenarios, in which at least one of the shells is not completely cold, such a restriction does exist. If β_4 is smaller than the minimum value set by n_1, n_4, ϵ_1 and ϵ_4 , the ram pressure cannot compensate for the excess energy gained by thermalization at the shock front. In these cases, two shocks cannot form. Rather, similar to the relativistic case, a rarefaction wave will form, which will gradually modify the properties of one of the shells.

3. Numerical Solution

In order to validate the analytical approximations presented in Section 2 above as well as to investigate the intermediate velocity (trans-relativistic) regime, we wrote a numerical code that solves the dynamical conditions at each of the four regimes - unshocked and shocked plasma shells that follow the collision of two plasma shells. The code simultaneously solves the set of twelve coupled equations: three shock jump conditions each for the forward and reverse shock waves, equating the pressure and velocity along the contact discontinuity and four equations of state. The results are obtained for a given set of six initial conditions: velocity, number and energy densities in regions (1) and (4), the unshocked plasmas.

3.1. Determination of the adiabatic indices in the different regimes

In order to account for the energy dependence of the adiabatic indices $\hat{\gamma}_i$ in each of the four regimes, we use the prescription derived by Service (1986), which is accurate to 10^{-5} . Since the classical gas law, $p_i = n_i T_i$ holds exactly in all regimes, one can write

$$\frac{e_i}{n_i} = T_i \left(\frac{e_i + p_i}{p_i} - 1 \right). \quad (18)$$

We use the approximation derived by Service (1986),

$$\frac{p_i}{e_i + p_i} = 0.36y + 0.036346y^2 - 0.088763y^3 - 0.047698y^4 - 0.083547y^5 + 0.073662y^6, \quad (19)$$

where

$$y \equiv \frac{T_i}{0.36 + T_i}. \quad (20)$$

The results of Equation 19 are tabulated. Thus, for a given ratio e_i/n_i , we use the tabulated results in Equation 18 to infer the temperature T_i in region i .

Once the temperature is known, at a second step the adiabatic index in each regime is calculated using

$$\hat{\gamma}_i = \frac{1}{3} (5 - 1.21937z + 0.18203z^2 - 0.96583z^3 + 2.32513z^4 - 2.39332z^5 + 1.07136z^6) \quad (21)$$

where

$$z \equiv \frac{T_i}{0.24 + T_i}. \quad (22)$$

Calculation of the dynamical properties of the plasmas in the different regimes is done as follows. We first guess a value of the shocked plasma velocity (more precisely, of $\Gamma_2\beta_2 = \Gamma_3\beta_3$), and solve for the two shock jump conditions. The value of $\Gamma_2\beta_2$ is then varied, until the pressures at each side of the contact discontinuity are equal.

In order to determine the adiabatic index in the shocked regions, for each value of $\Gamma_2\beta_2$ the shock jump conditions are solved in iterative way. Following an initial guess of $\hat{\gamma}_2, \hat{\gamma}_3$, the shock jump conditions are solved and the values of the specific energies e_2/n_2 and e_3/n_3 are determined. The values of the adiabatic index are then re-calculated, and the calculation is repeated with the new value. We found that convergence is typically very quick, within few iterations at most.

3.2. Numerical results

Examples of the numerical results, together with the analytical approximations in the different regimes are presented in Figures 1 – 3.

In Figure 1, we calculate the dynamical and thermal properties in all four regimes following the collision of two cold plasma shells. The first (slow) shell is characterized by density $n = 1 \text{ cm}^{-3}$ and zero internal energy ($e_1 = n_1 m_e c^2$). The fast plasma shell is characterized by higher density of $n_4 = 100 \text{ cm}^{-3}$ and is similarly cold, $e_4 = n_4 m_e c^2$. The density contrast is chosen to be 100 for presentation purposes. We further chose the slow plasma to be motionless, $\beta_1 = 1$. The results are presented as a function of $\Gamma_4 \beta_4$, where β_4 is the relative velocity between the shells.

For cold plasmas as considered in Figure 1, there is no lower limit on β_4 , i.e., the two shock system always forms, for any value of $\beta_4 > 0$. This system of cold plasmas is in fact identical to the one considered already by Sari & Piran (1995). In Figure 1(a) we show the shocked plasma velocity, $(\Gamma_2 \beta_2)$, in the rest frame of the slow shell as well as the same velocity in the rest frame of the unshocked, fast plasma in region (4), denoted by $(\bar{\Gamma}_3 \bar{\beta}_3)$. The asymptotic approximations in the relativistic (Equations 8) and non-relativistic (Table 1 (a)) regimes are given by the dashed and dash-dotted lines. In producing the non-relativistic approximation of the velocities, we replace β_4 with $\Gamma_4 \beta_4$. The results show excellent agreement - better than $\sim 10\%$ for $\Gamma_4 \beta_4 \leq 2$.

In Figures 1(b) and 1(c) we show the energy densities and the energy per particle (e_i/n_i) in the shocked plasma regions (2) and (3) as a function of $\Gamma_4 \beta_4$. The analytic approximations in the relativistic regime (Equation 9) and non-relativistic regime (Equation 17) again provide an excellent description of the thermodynamical properties of the plasma. The transition between the non-relativistic and relativistic regimes occurs for those values of $\Gamma_4 \beta_4$ in which $\Gamma_2 \beta_2 / \bar{\Gamma}_3 \bar{\beta}_3$ becomes relativistic. Finally, in Figure 1(d) we show the adiabatic indices in the different regimes. While clearly $\hat{\gamma}_1 = \hat{\gamma}_4 = 5/3$, the adiabatic indices of the shocked plasma are gradually changing as $\Gamma_4 \beta_4$ increases, and the shocked plasma heats.

In Figure 2 we consider a more complicated scenario, that of a collision between two cool shells. We chose as parameters $n_1 = 99.99 \text{ cm}^{-3}$, $\epsilon_1 = 0.01 \text{ erg cm}^{-3}$ (namely, $e_1 = 100 \text{ erg cm}^{-3}$), $n_4 = 4.99 \text{ cm}^{-3}$ and $\epsilon_4 = 0.01 \text{ erg cm}^{-3}$. Similar to the previous example, we took $\beta_1 = 0$, namely slow shell at rest. These values are chosen for presentation purposes, as we want to ensure a good contrast of the shocked plasma properties between the different regimes.

The velocities of the shocked plasma regions (2) and (3) as measured in the rest frames of the slow plasma shell ($\Gamma_2 \beta_2$) and the fast plasma shell ($\bar{\Gamma}_3 \bar{\beta}_3$) are shown in Figure 2(a).

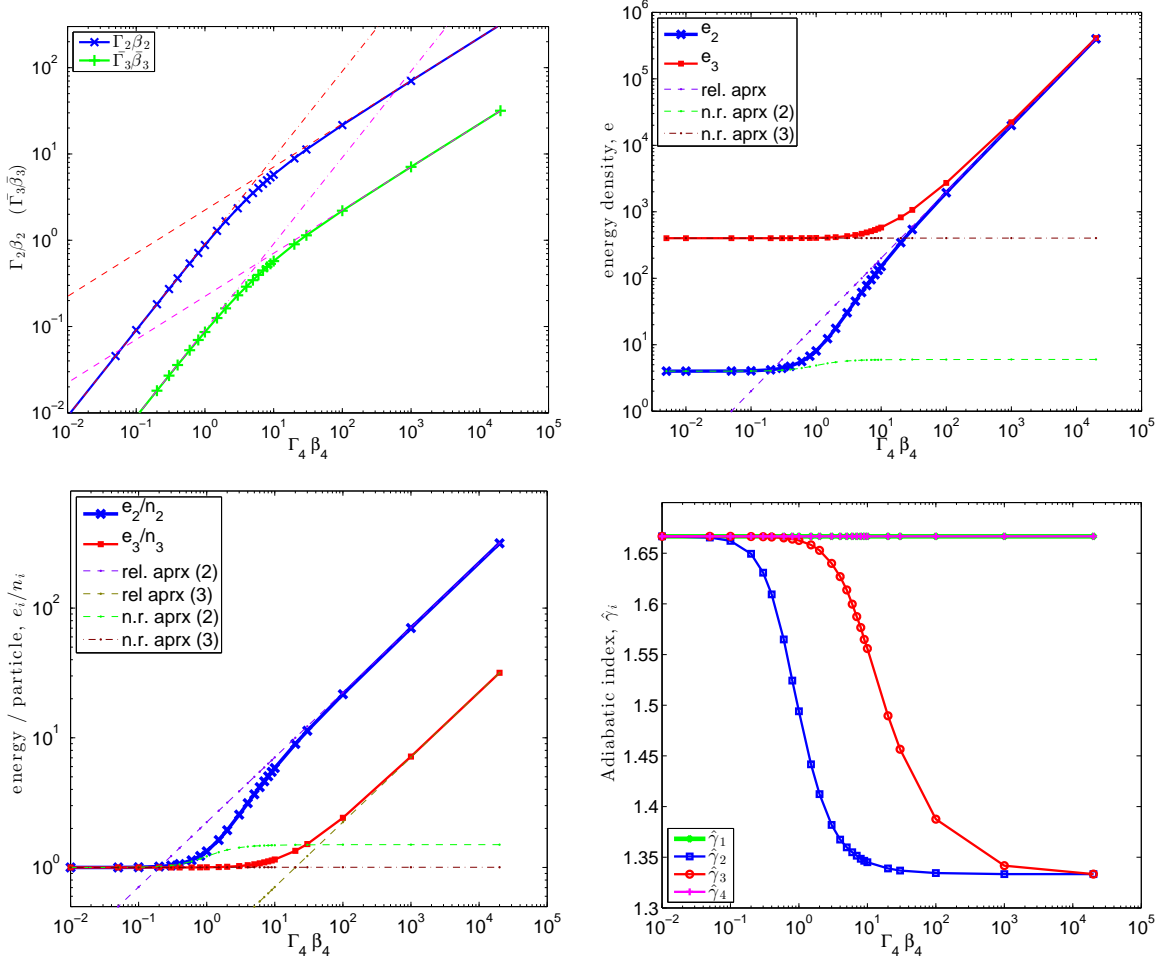


Fig. 1.— Velocities and thermodynamic properties of the shocked plasma following collision between two cold plasma shells ($\epsilon_i = 0$, $i = 1, 4$). Parameters considered are $n_1 = 1 \text{ cm}^{-3}$, $\epsilon_1 = 0$, $n_4 = 100 \text{ cm}^{-3}$, $\epsilon_4 = 0$, $\beta_1 = 0$. Plasma parameters are shown as a function of the fast shell initial velocity, $\Gamma_4\beta_4$. Top left (a): Velocities of the shocked plasma regions (2) and (3), as measured in the rest frame of slow plasma shell in region (1) ($\Gamma_2\beta_2$) and the rest frame of the fast plasma shell in region (4), ($\bar{\Gamma}_3\bar{\beta}_3$). Top right (b): Energy densities in the shocked plasma regions (2) and (3). Bottom left (c): Energy per particle, e_i/n_i in the shocked plasma regions (2) and (3). Bottom right (d): Adiabatic indices $\hat{\gamma}_i$ in the four different regimes.

The analytical approximation in the relativistic regime (Equation 8) and the non-relativistic regime (Table 1 (d)) provide excellent approximations in the two regimes. The decay of the analytical approximation to $\bar{\beta}_3 = \beta_4 - \beta_2$ around $\Gamma_4 \sim 1$ arises from the use of $\Gamma_4\beta_4$ in the calculation of β_2 .

The ratio of densities across the forward shock is shown in Figure 2(b), together with the analytic approximations. There are clearly three distinct regimes. First, there is the relativistic regime, $\Gamma_2 \gg 1$. In this regime, the density ratio is well approximated by the results given in Equation 7. A second regime is the non-relativistic, “cold” regime, namely $\beta_2 \geq \sqrt{2\epsilon_1/n_1} = 0.014$ (in the considered scenario), in which the density ratio is well approximated by Equation 17. Finally, when $\beta_2 \ll \sqrt{2\epsilon_1/n_1}$, the approximation in the “cool” regime given in Equation 16 provides a good fit to the density ratio. These same three regimes are also clearly observed when considering the energy densities of the shocked plasma in Figure 2(c). Interestingly, when considering the ratio e_i/n_i (Figure 2(d)) in the non-relativistic regime, the cool and cold approximations can be combined to provide a good approximation which reads $e_2/n_2 \simeq 1 + (\epsilon_1/n_1) + (\Gamma_2\beta_2)^2/2$. In the relativistic regime, this ratio is well described by Equation 9.

In Figure 3 we provide a third example, that of a collision between two initially hot plasma shells. As initial parameters, we chose $n_1 = 1 \text{ cm}^{-3}$, $e_1 = 15 \text{ erg cm}^{-3}$, $n_4 = 1 \text{ cm}^{-3}$, $e_4 = 10 \text{ erg cm}^{-3}$ and $\beta_1 = 0$.

For this choice of parameters, the results of Table 1 (f) show a minimum value of β_4 , below which two shock waves cannot form: For $\beta_4 = \sqrt{3}(\epsilon_1 - \epsilon_4)/4\epsilon_4 \simeq 0.24$, $\beta_2 \rightarrow 0$. This is clearly demonstrated in Figure 3(a). At larger relative velocity, the results in Equation 8 and Table 1 (f) provide an excellent approximation to the shocked plasma velocity. The ratio of number densities across the forward shock, n_2/n_1 (Figure 3(b)) is well approximated by the analytical approximations in Equation 7 (relativistic) and 13 (non-relativistic). Similarly, the energy per particle in the shocked regions (2) and (3) shown in Figure 3(c) are well approximated by the analytical result in Equation 9 in the relativistic regime, and by $e_2/n_2 \simeq (e_1/n_1)(1 + \Gamma_2\beta_2/\sqrt{3} + (\Gamma_2\beta_2)^2/6)$ in the non-relativistic regime, which is readily derived from Equations 13 and 14.

4. Observational Consequences

4.1. Efficiency in kinetic energy dissipation

The calculations above enable us to determine the efficiency of kinetic energy conversion during two shell collisions. Various authors have calculated this efficiency using an integral

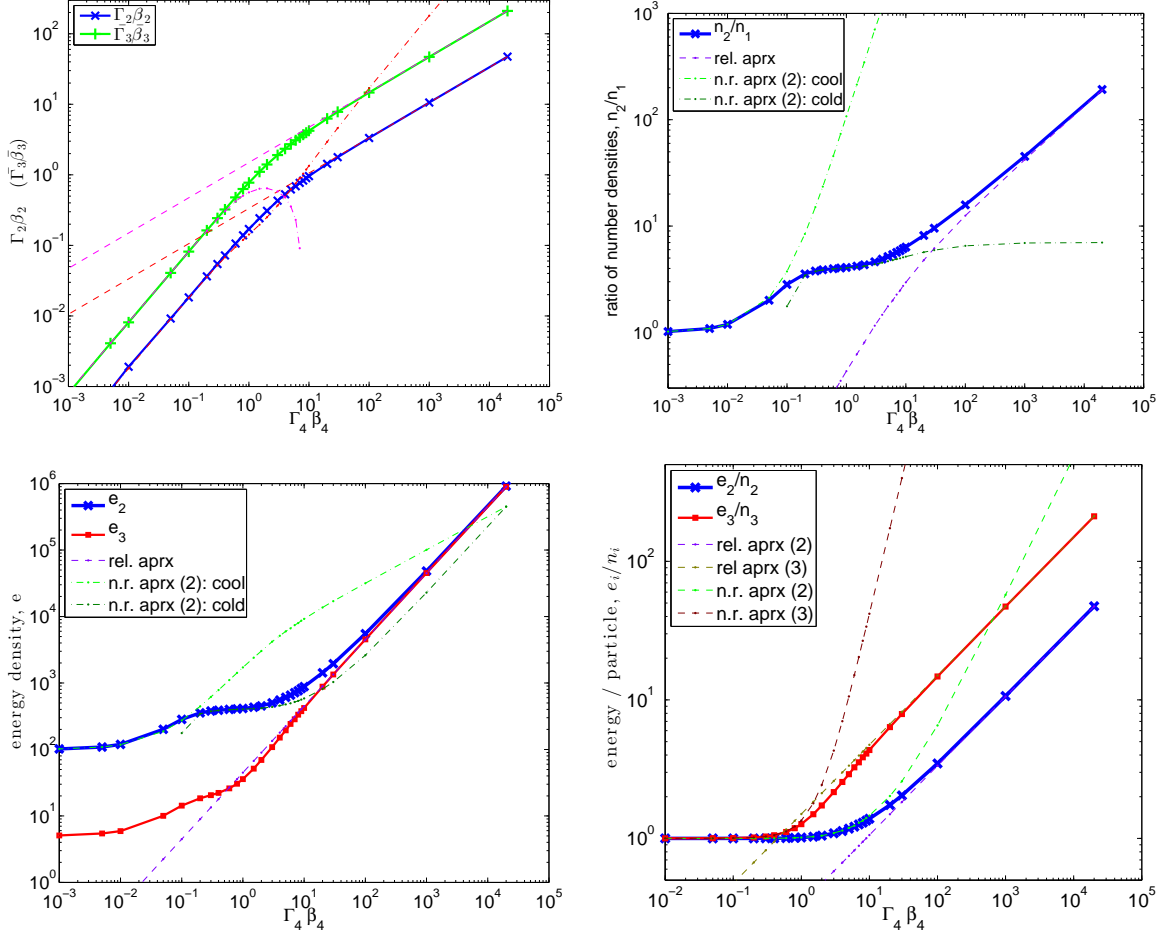


Fig. 2.— Velocities and thermodynamic properties of the shocked plasma following collision between two cool plasma shells ($\epsilon_i/n_i \ll 1$, $i = 1, 4$). Parameters considered are $n_1 = 99.99 \text{ cm}^{-3}$, $\epsilon_1 = 0.01 \text{ erg cm}^{-3}$, $n_4 = 4.99 \text{ cm}^{-3}$, $\epsilon_4 = 0.01 \text{ erg cm}^{-3}$, $\beta_1 = 0$. Plasma parameters are shown as a function of the fast shell initial velocity, $\Gamma_4 \beta_4$. Top left (a): Velocities of the shocked plasma (same as in Figure 1)(a), for collision of cool plasma shells. Top Right (b): Ratio of number densities across the forward shock, n_2/n_1 . Bottom left (c): Energy densities in the shocked plasma regions (2) and (3). Bottom right (d): Energy per particle, e_i/n_i in the shocked plasma regions (2) and (3).

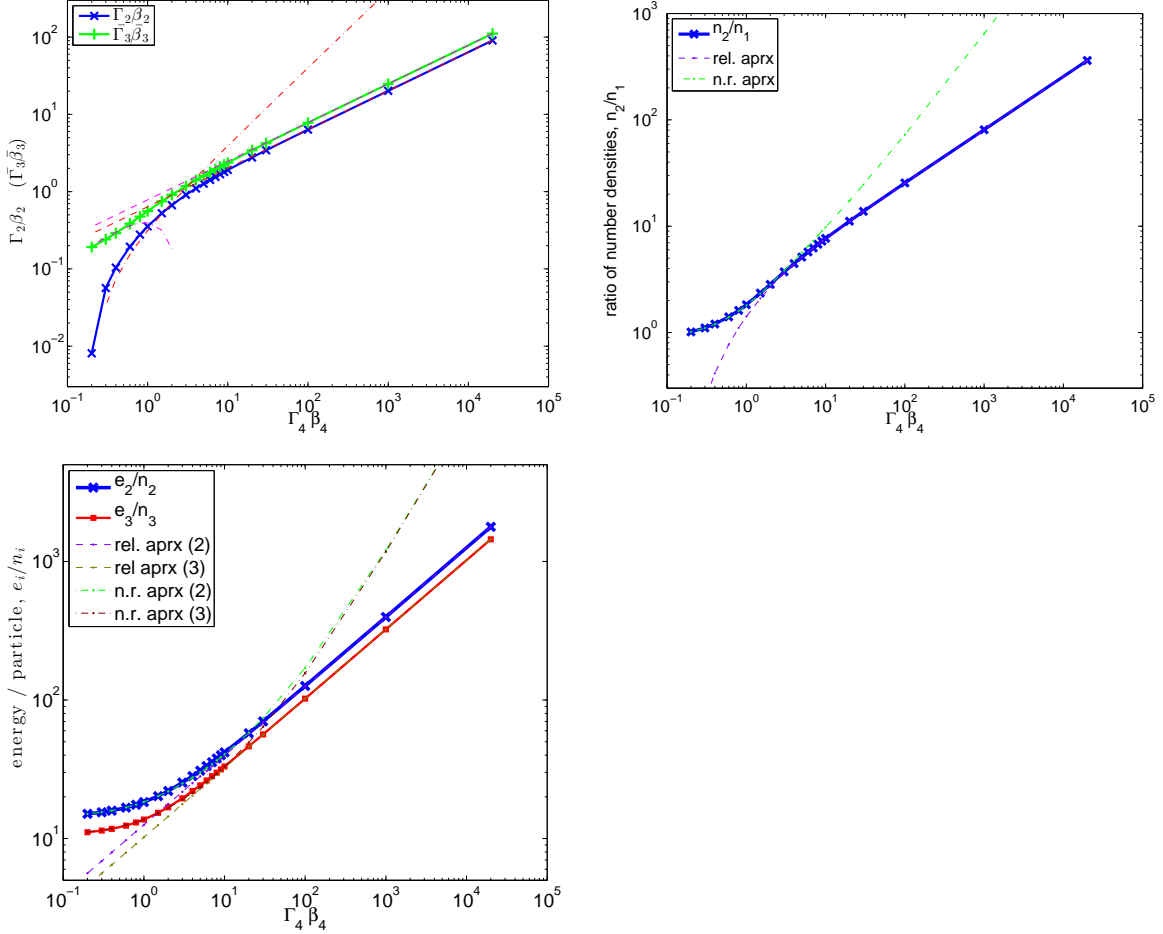


Fig. 3.— Velocities and thermodynamic properties of the shocked plasma following collision between two initially hot ($e_i/n_i \gg 1$) plasma shells. Parameters considered are $n_1 = 1 \text{ cm}^{-3}$, $e_1 = 15 \text{ erg cm}^{-3}$, $n_4 = 1 \text{ cm}^{-3}$, $e_4 = 10 \text{ erg cm}^{-3}$, $\beta_1 = 0$. Plasma parameters are shown as a function of the fast shell initial velocity, $\Gamma_4 \beta_4$. Top left (a): Velocities of the shocked plasma (same as in Figure 1(a)), for collision of two hot plasma shells. Top right (b): Ratio of number densities across the forward shock, n_2/n_1 . Bottom left (c): Energy per particle, e_i/n_i in the shocked plasma regions (2) and (3).

approach, namely by determining the merged shell bulk Lorentz factor assuming a plastic collision between the two shells, and using conservations of energy and momentum. For example, Kobayashi et al. (1997) and Malzac (2014) considered cold plasma shells, while Spada et al. (2001) and Jamil et al. (2010) generalized the result to hot plasmas.

Using the formulation developed here, we can generalize these results. The calculation is done in the rest frame of the shocked plasma. In this frame, the slow shell in region (1) is seen to have a Lorentz factor $\tilde{\Gamma}_1$ (corresponding velocity $\tilde{\beta}_1$), where $\tilde{\Gamma}_1\tilde{\beta}_1 = \Gamma_1\Gamma_2(\beta_1 - \beta_2)$. The transfer of momentum from the slow shell (region (1)) to the shocked plasma (region (2)), assuming a planar symmetry along the x direction is given by

$$dP^x(1) = \int dV'_1 T^{01} = \int dV'_1 \omega_1 \tilde{\Gamma}_1^2 \tilde{\beta}_1 = \int dV_1 \omega_1 \tilde{\Gamma}_1 \tilde{\beta}_1. \quad (23)$$

Here, $dV'_1 = dV_1/\tilde{\Gamma}_1$ is the volume element of material in region (1) that crosses the forward shock into region (2) per unit time, as seen in the rest frame of shocked region (2), and dV_1 is the same volume element as measured in the rest frame of region (1).

Using $\omega_1 = n_1 + \hat{\gamma}_1 \epsilon_1$, as well as $dM_1 = \int dV_1 n_1$ and $dE_{th,1} = \int dV_1 \epsilon_1$, the momentum transfer rate can be written as

$$dP^x(1) = (dM_1 + \hat{\gamma}_1 dE_{th,1}) \tilde{\Gamma}_1 \tilde{\beta}_1, \quad (24)$$

where we assumed that the velocities are not changed during the shock propagation.

A similar calculation holds for the momentum transfer from the fast plasma (region (4)), which could be written as

$$dP^x(4) = (dM_4 + \hat{\gamma}_4 dE_{th,4}) \bar{\Gamma}_3 \bar{\beta}_3, \quad (25)$$

where $\bar{\Gamma}_3 \bar{\beta}_3 = \Gamma_4 \Gamma_2 (\beta_4 - \beta_2)$. Equating the momentum transfer in both sides leads to the velocity at the center of mass frame, which is the shocked fluid frame as long as both shockers exist,

$$\beta_2 = \frac{\Gamma_1 \beta_1 (dM_1 + \hat{\gamma}_1 dE_{th,1}) + \Gamma_4 \beta_4 (dM_4 + \hat{\gamma}_4 dE_{th,4})}{\Gamma_1 (dM_1 + \hat{\gamma}_1 dE_{th,1}) + \Gamma_4 (dM_4 + \hat{\gamma}_4 dE_{th,4})}. \quad (26)$$

In the ultra-relativistic case, $\Gamma_4 \gg \Gamma_2 \gg 1$ this can be written as

$$\Gamma_2 \simeq \left(\frac{\Gamma_1 (dM_1 + \hat{\gamma}_1 dE_{th,1}) + \Gamma_4 (dM_4 + \hat{\gamma}_4 dE_{th,4})}{(dM_1 + \hat{\gamma}_1 dE_{th,1})/\Gamma_1 + (dM_4 + \hat{\gamma}_4 dE_{th,4})/\Gamma_4} \right)^{1/2}. \quad (27)$$

This result differs from the result that appears in Spada et al. (2001) (their Equation (4)) as well as in Jamil et al. (2010), by the inclusion of the adiabatic indices $\hat{\gamma}_i$ that multiply

the thermal energies, which are omitted in these works. These can be traced back to the inclusion of the pressure term in the shocked plasma.

We further point out that equating the momenta transfer from regions (1) and (4) using equations 24 and 25 in the relativistic case, would retrieve back Equation 8. These results imply that the efficiency of kinetic energy conversion as calculated in Spada et al. (2001) and Jamil et al. (2010) hold, provided that the final Lorentz factor is calculated using Equation 27.

4.2. Basic scalings of synchrotron emission

The heated shocked plasma will radiate its energy. The observed signal can therefore be used as a probe of the initial, unshocked plasma shells properties. Full radiative calculations require additional parameters, such as the exact value of the magnetic field as well as assumptions about the radiating particles distribution in the shocked plasma regions, and are therefore left for a future work.

Here, we provide some basic scaling laws of the characteristic frequencies expected from synchrotron emission, which is likely the easiest (and most commonly discussed) signal that can be detected, and can therefore be used to probe the plasma conditions. These are particularly simple in the relativistic regime, where the plasma is substantially heated by the shock waves. We therefore focus here in the relativistic regime.

We scale the properties of the synchrotron emission in region i by adopting the common assumption that magnetic fields are generated by the shock waves, and that the generated magnetic energy density is some constant fraction of the post-shock thermal energy density, namely $B_i^2 \propto e_i$. Furthermore, we assume that the electrons carry some constant fraction of the proton energy, resulting in electron's Lorentz factor $\gamma_{el,i} \propto (e_i/n_i)$. As the characteristic synchrotron emission frequency is $\nu_{syn,i} \propto B_i \gamma_{el,i}^2$, one finds the scaling

$$\frac{\nu_{syn,2}}{\nu_{syn,3}} \propto \frac{e_2^{1/2} \left(\frac{e_2}{n_2}\right)^2}{e_3^{1/2} \left(\frac{e_3}{n_3}\right)^2} = \left(\frac{n_4}{n_1}\right)^2 \left(\frac{\omega_1}{\omega_4}\right). \quad (28)$$

If we denote by Δ_1 and Δ_4 the (comoving) widths of the colliding shells, the total number of radiating electrons is $N_1 \propto n_1 \Delta_1$ and $N_4 \propto n_4 \Delta_4$ (under the 1-d assumption). Since the total observed power is $P_{syn} \propto NB^2 \gamma_{el}^2$ (Rybicki & Lightman 1979), the ratio of

synchrotron power between the two shocked regions is therefore

$$\frac{P_{syn,2}}{P_{syn,3}} = \frac{n_1 \Delta_1 e_2 \left(\frac{e_2}{n_2}\right)^2}{n_4 \Delta_4 e_3 \left(\frac{e_3}{n_3}\right)^2} = \left(\frac{\Delta_1}{\Delta_4}\right) \left(\frac{n_4}{n_1}\right) \left(\frac{\omega_1}{\omega_4}\right). \quad (29)$$

In the relativistic scenario, the observed time scale for the forward shock wave to cross the slow plasma shell is $\sim \Delta_1 \Gamma_1 / c$, while the time scale of the reverse shock to cross the fast plasma is $\approx \Delta_4 \Gamma_2^2 / \Gamma_4 c \sim 2 \Gamma_1 (\omega_4 / \omega_1) \Delta_4 c$ (e.g., Sari & Piran 1995). Thus, the observed ratio of the time scale of existence of the two shock waves is

$$\frac{t_{fs}}{t_{rs}} = \left(\frac{\Delta_1}{\Delta_4}\right) \left(\frac{\omega_1}{\omega_4}\right). \quad (30)$$

These results imply that identification of the ratios of the three main characteristics of synchrotron emission from the forward and reverse shock waves, namely the characteristic frequency, total power and time scales, are sufficient to provide direct information about the ratio of number densities, enthalpies and initial sizes of the colliding shells. Interestingly, in the ultra-relativistic limit, these results are independent on the unknown Lorentz factor. As we showed above, using these initial conditions one can calculate the properties of the merged shell. Therefore, direct observations of multiple shell collisions could provide information about two key ingredients. The first is the initial conditions of the ejected shells, hence the properties of the inner engine. The second is the temporal, hence spatial evolution (adiabatic losses) of the merged shell.

5. Summary and discussion

In this work, we considered the collision of two plasma shells, as is expected in the “internal shock” model. We generalized previous treatments of the problem by considering plasmas which can be arbitrarily hot. This is a natural consequence of the internal shocks scenario, as, after the first collision, the merged shell is inevitably hot (and can be very hot if the shells are relativistic, see Equation 9). We point out that while in between collisions the colliding shells lose their energy adiabatically, the decrease in temperature (or energy per particle) is $(e/n) \propto T \propto r^{-2/3}$, and thus even if the internal collisions occur within a range of several orders of magnitude in radii, adiabatic cooling is not sufficient to completely cool the plasma shells.

We derived analytical approximations for the shocked shell velocities in both the relativistic (Equation 8) and non-relativistic (Table 1) regimes. A very important result we found

is that in the general scenario (as opposed to the cold scenario) there is a minimum relative velocity, or Lorentz factor, that enables the formation of the two shock system (Equation 10). The physical reason for this is the requirement of the ram pressure to exceed the pressure associated with the excess of thermal energy caused by the shock. If this criterion is not met, only a single shock wave is expected, while a rarefaction wave will propagate into the hotter plasma. In this case, we expect the radiative signal to be much weaker.

We further provided analytical expressions for the energy density and for the energy per particle in the shocked region. We found that for non-relativistic collision, one needs to discriminate between three scenarios: “hot” plasma, for which $\epsilon/n \gg 1$, “cool” plasmas for which $1 \gg \epsilon/n \gg \beta^2$, and “cold” plasma, for which $1 \gg \beta^2 \gg \epsilon/n$. We provided the analytical expressions for the shocked plasma thermodynamical properties in each of these cases.

We discussed several observational consequences of the dynamical results. We showed that in calculating the final Lorentz factor of the merged shell, hence the efficiency of kinetic energy dissipation, one needs to consider the pressure of the shocked plasma. We provided the basic scaling laws of synchrotron emission in the ultra-relativistic regime, and showed that measurements of the peak energy, flux and time scale of emission enables one to deduce important information about the initial shells properties, as well as the spatial evolution of the propagating shells.

The results provided here emphasise the fact that the properties of the shocked plasma depend not only on the relative velocities between the colliding plasma shells, but also on the energy per particle in each colliding shell. These results are therefore important in the study of signals from multiple collisions that are expected in various environments, such as GRBs, XRBs and AGNs. Furthermore, our numerical results are particularly useful for probing the plasma properties in the trans-relativistic regime, which is likely the dominant regime in XRBs and possibly AGNs. As we demonstrated in §3 above, while no simple analytical expressions exist in this regime, still reasonable analytical fits do exist, and can be very useful in understanding the underlying properties of these objects.

AP wishes to thank Damien Bégué, Felix Ryde, Ralph Wijers and Bing Zhang for useful comments. This research was partially supported by the European Union Seventh Framework Programme (FP7/2007-2013) under grant agreement n° 618499.

REFERENCES

- Beloborodov, A. M. 2000, *ApJ*, 539, L25
- Blandford, R. D. & McKee, C. F. 1976, *Physics of Fluids*, 19, 1130
- Böttcher, M. & Dermer, C. D. 2010, *ApJ*, 711, 445
- Cantó, J., Lizano, S., Fernández-López, M., González, R. F., & Hernández-Gómez, A. 2013, *MNRAS*, 430, 2703
- Daigne, F. & Mochkovitch, R. 1998, *MNRAS*, 296, 275
- Drappeau, S., Malzac, J., Belmont, R., Gandhi, P., & Corbel, S. 2015, *MNRAS*, 447, 3832
- Fender, R. P. 2001, *MNRAS*, 322, 31
- Fenimore, E. E., Madras, C. D., & Nayakshin, S. 1996, *ApJ*, 473, 998
- Ghisellini, G. 1999, *Astronomische Nachrichten*, 320, 232
- Guetta, D., Spada, M., & Waxman, E. 2001, *ApJ*, 557, 399
- Jamil, O., Fender, R. P., & Kaiser, C. R. 2010, *MNRAS*, 401, 394
- Kaiser, C. R., Sunyaev, R., & Spruit, H. C. 2000, *A&A*, 356, 975
- Kino, M., Mizuta, A., & Yamada, S. 2004, *ApJ*, 611, 1021
- Kobayashi, S., Piran, T., & Sari, R. 1997, *ApJ*, 490, 92
- Malzac, J. 2013, *MNRAS*, 429, L20
- . 2014, *MNRAS*, 443, 299
- Marscher, A. P. 1980, *ApJ*, 235, 386
- Mészáros, P., Ramirez-Ruiz, E., Rees, M. J., & Zhang, B. 2002, *ApJ*, 578, 812
- Miller-Jones, J. C. A., McCormick, D. G., Fender, R. P., Spencer, R. E., Muxlow, T. W. B., & Pooley, G. G. 2005, *MNRAS*, 363, 867
- Mimica, P. & Aloy, M. A. 2010, *MNRAS*, 401, 525
- Nakar, E. & Piran, T. 2002, *ApJ*, 572, L139

- Norris, J. P., Nemiroff, R. J., Bonnell, J. T., Scargle, J. D., Kouveliotou, C., Paciesas, W. S., Meegan, C. A., & Fishman, G. J. 1996, *ApJ*, 459, 393
- Panaitescu, A., Spada, M., & Mészáros, P. 1999, *ApJ*, 522, L105
- Pe’er, A. 2014, *Space Sci. Rev.*, 183, 371
- Ramirez-Ruiz, E. & Fenimore, E. E. 2000, *ApJ*, 539, 712
- Rees, M. J. 1978, *MNRAS*, 184, 61P
- Rees, M. J. & Meszaros, P. 1994, *ApJ*, 430, L93
- Rybicki, G. B. & Lightman, A. P. 1979, *Radiative processes in astrophysics*
- Sari, R. & Piran, T. 1995, *ApJ*, 455, L143
- . 1997, *ApJ*, 485, 270
- Service, A. T. 1986, *ApJ*, 307, 60
- Sikora, M., Begelman, M. C., & Rees, M. J. 1994, *ApJ*, 421, 153
- Spada, M., Ghisellini, G., Lazzati, D., & Celotti, A. 2001, *MNRAS*, 325, 1559
- Wang, F. Y. & Cheng, K. S. 2012, *MNRAS*, 421, 908
- Wiersma, J. 2007, PhD thesis, Utrecht University
- Zhang, B. & Mészáros, P. 2002, *ApJ*, 566, 712

Table 1. Shocked plasma velocities in the various cases.

Scenario	Shocked shell velocities, $\beta_2 = \beta_3$
(a) cold \rightarrow cold	$\beta_4 \frac{\sqrt{\frac{n_4}{n_1}}}{\sqrt{\frac{n_4}{n_1} + 1}}$
(b) cold \rightarrow cool	$\beta_4 - \left[\frac{1}{2} \left(\frac{\hat{\gamma}_2 - 1}{\hat{\gamma}_3 - 1} \right) \left(\frac{n_1}{n_4} \right) \left(\frac{\epsilon_1}{n_1} \right) \right]^{1/2}$
(c) cold \rightarrow hot	same as (b), cold \rightarrow cool
(d) cool \rightarrow cool	$\frac{(\hat{\gamma}_3 - 1)\epsilon_4 - (\hat{\gamma}_2 - 1)\epsilon_1 + (\hat{\gamma}_3 - 1)\sqrt{\frac{\hat{\gamma}_4}{\hat{\gamma}_4 - 1}}\sqrt{n_4\epsilon_4}\beta_4}{(\hat{\gamma}_2 - 1)\sqrt{\frac{\hat{\gamma}_1}{\hat{\gamma}_1 - 1}}\sqrt{n_1\epsilon_1} + (\hat{\gamma}_3 - 1)\sqrt{\frac{\hat{\gamma}_4}{\hat{\gamma}_4 - 1}}\sqrt{n_4\epsilon_4}}$
(e) cool \rightarrow hot	$\frac{(\hat{\gamma}_3 - 1)\epsilon_4 - (\hat{\gamma}_2 - 1)\epsilon_1 + (\hat{\gamma}_3 - 1)\sqrt{\frac{\hat{\gamma}_4}{\hat{\gamma}_4 - 1}}\sqrt{n_4\epsilon_4}\beta_4}{(\hat{\gamma}_2 - 1)\frac{4}{\sqrt{3}\epsilon_1} + (\hat{\gamma}_3 - 1)\sqrt{\frac{\hat{\gamma}_4}{\hat{\gamma}_4 - 1}}\sqrt{n_4\epsilon_4}}$
(f) hot \rightarrow hot	$\frac{\epsilon_4 - \epsilon_1 + \frac{4}{\sqrt{3}}\epsilon_4\beta_4}{\frac{4}{\sqrt{3}}(\epsilon_1 + \epsilon_4)}$